A numerical study of elastic bodies that are described by constitutive equations that exhibit limited strains

A. Ortiz-Bernardin [a,*], R. Bustamante [a], K.R. Rajagopal [b]

[a] *Department of Mechanical Engineering, University of Chile, Beauchef 850, Santiago 8370448, Chile*
[b] *Department of Mechanical Engineering, Texas A & M University, College Station, TX 77843, USA*

ABSTRACT

Recently, a very general and novel class of implicit bodies has been developed to describe the elastic response of solids. It contains as a special subclass the classical Cauchy and Green elastic bodies. Within the class of such bodies, one can obtain through a rigorous approximation, constitutive relations for the linearized strain as a nonlinear function of the stress. Such an approximation is not possible within classical theories of Cauchy and Green elasticity, where the process of linearization will only lead to the classical linearized elastic body.

In this paper, we study numerically the states of stress and strain in a finite rectangular plate with an elliptic hole and a stepped flat tension bar with shoulder fillets, within the context of the new class of models for elastic bodies that guarantees that the linearized strain would stay bounded and limited below a value that can be fixed a priori, thereby guaranteeing the validity of the use of the model. This is in contrast to the classical linearized elastic model, wherein the strains can become large enough in the body leading to an obvious inconsistency.

© 2013 Elsevier Ltd. All rights reserved.

1. Introduction

Recently, a new class of implicit constitutive relations was introduced to describe the response of elastic bodies (see Rajagopal, 2003, 2007, 2011b, Rajagopal and Srinivasa, 2007, 2009 and Bustamante, 2009). This new class includes the explicit theories of Cauchy elasticity and Green elasticity as special subclasses. The advantages that such models provide over the classical models are detailed in several papers (Rajagopal, 2011b,a; Bustamante and Rajagopal, 2010) and hence we shall not repeat them here. Suffice it is to say that very important problems such as the problem of fracture, which has defied a proper consistent explanation without resorting to ad hoc procedures (see Rajagopal and Walton, 2011, Kulvait et al., 2013, Ortiz et al., 2012, and Bulíček et al., 2013 with regard to how the problem is dealt within the context of the new class of models) and the modeling of certain phenomena exhibited by soft material that has hitherto defied explanation within the context of classical models (see the discussion in Freed and Einstein (2013a,b); Freed et al., 2013) are some examples of the potential of the new class of implicit constitutive relations. The class of implicit models has also been extended to develop models to describe the electroelastic response of bodies and it has been able to describe phenomena that have thus far been impossible

to explain within the context of classical electroelastic theories (see Bustamante and Rajagopal, 2013b,a).

Another special subclass of the implicit models for elasticity introduced by Rajagopal (2003) is explicit models for the stretch in terms of the stress (see Rajagopal, 2007, 2011b) and its linearization that leads to an explicit nonlinear expression for the linearized strain in terms of the stress. The latter class of models is impossible within the context of classical theories of elasticity and this paper is concerned with a study of such models (see the model defined through (15)). When one is concerned with constitutive relations for the Cauchy–Green stretch or the linearized strain in terms of the stress, one does not have the luxury of substituting the expression for the stress in terms of the displacement gradient into the balance of linear momentum and obtaining a partial differential equation for the displacement field. Instead, the constitutive relation, the balance of linear momentum, and whatever other balance laws are relevant, need to be solved simultaneously; hence the stress and displacement fields are both unknowns that need to be solved for. This system of coupled nonlinear partial differential equations is far more daunting than the much simplified system that is obtained when an explicit expression for the stress in terms of the displacement gradient can be substituted into the balance of linear momentum. In this study, we are concerned with an explicit expression for the linearized strain in terms of the stress and hence concerned with the more complex system of coupled partial differential equations.

* Corresponding author. Tel.: +56 (2) 297 846 64; fax: +56 (2) 268 960 57.
E-mail address: aortizb@ing.uchile.cl (A. Ortiz-Bernardin).

Though the system is complicated in that the number of equations to be solved is larger, the order of the equations within the purview of the new framework is a system of lower order equations and thus from the point of view of numerical analysis provides some advantages.

Most of the studies until recently have been concerned with special boundary value problems, in infinite domains, wherein semi-inverse assumptions are made to reduce the problem to the study of much simplified governing equations, which in most instances is a system of ordinary differential equations. In this paper, we shall study problems in finite domains and as it is unlikely that we can simplify the problem to obtain simpler ordinary differential equations, we shall have to study the problem numerically. We will study two problems, that of the stress concentration due to the presence of an elliptic hole and that of the stress concentration in a stepped flat tension bar with shoulder fillets, within the context of the new class of models. The first of the two problems has relevance to the problem of stress concentration due to a crack as such a situation can be achieved by taking the limit of the ratio of the minor axis to the major axis of the elliptic hole to tend to zero.

The organization of the paper is as follows. In Section 2, we introduce the basic kinematics, document the general implicit constitutive relation between the stress and the stretch for isotropic bodies, and derive a special constitutive relation for the linearized strain in terms of the stress under the assumption that the displacement gradient is small. We then record some special constitutive expressions for the linearized strain in terms of the stress and develop the system of governing equations that need to be solved. In Section 3, the necessary weak and linearized weak forms are presented and the linearized weak form is discretized using the finite element method. The computational method and algorithms are discussed in Section 4. Finally, Section 5 is devoted to a discussion of the numerical results. In the case of the problem of a plate with an elliptic hole subjected to tension with the applied tension being perpendicular to the major axis, we find (as is to be expected) that the strains are maximum at the vertices along the major axis; however they remain bounded below the value for which the linearization is valid even as the stress increases. In the case of the stepped flat tension bar with shoulder fillets, the strain is maximum at the shoulder but once again remains below the value that guarantees the validity of the linearization.

Unlike the classical linearized model which leads to ever increasing strains that make the model that is being used invalid, the current study is a consistent approach that guarantees that the model that is being used is applicable throughout the domain of application of the model. This fact cannot be overemphasized.

2. Basic equations

2.1. Kinematics

Let $X \in \mathcal{B}$ denote a point in an abstract body $\mathcal{B}$ and $\mathbf{X} = \boldsymbol{\kappa}(X)$ the position of X in the reference configuration $\kappa_r(\mathcal{B})$; we assume there exists a one-to-one function $\boldsymbol{\chi}$ referred to as the motion of the body such that $\mathbf{x} = \boldsymbol{\chi}(\mathbf{X}, t)$, where $\mathbf{x}$ is the position of X in the current configuration $\kappa_t(\mathcal{B})$ at time t.

The deformation gradient $\mathbf{F}$ and the right and the left Cauchy–Green strain tensors, $\mathbf{C}$ and $\mathbf{B}$, are defined as

$$\mathbf{F} = \frac{\partial \mathbf{x}}{\partial \mathbf{X}}, \quad \mathbf{C} = \mathbf{F}^{\mathrm{T}}\mathbf{F}, \quad \mathbf{B} = \mathbf{F}\mathbf{F}^{\mathrm{T}}, \tag{1}$$

respectively. The displacement field $\mathbf{u}$ is defined through

$$\mathbf{u} = \mathbf{x} - \mathbf{X}. \tag{2}$$

Finally, the Green–St. Venant strain ($\mathbf{E}$) and the linearized strain ($\boldsymbol{\varepsilon}$) are defined through

$$\mathbf{E} = \frac{1}{2}(\mathbf{F}^{\mathrm{T}}\mathbf{F} - \mathbf{I}), \quad \boldsymbol{\varepsilon} = \frac{1}{2}[\nabla\mathbf{u} + (\nabla\mathbf{u})^{\mathrm{T}}]. \tag{3}$$

In this work, we consider the case $\|\nabla\mathbf{u}\| \sim O(\delta)$ with $\delta \ll 1$ and thus the relevant strain measure is the linearized strain. Hence, the current and the reference configuration are coincident.

2.2. Equilibrium equation and constitutive relations

In this paper, we study quasi-static problems in the absence of body forces. The equilibrium equation in terms of the Cauchy stress tensor $\boldsymbol{\sigma}$ is

$$\mathrm{div}\boldsymbol{\sigma} = \mathbf{0}. \tag{4}$$

For elastic bodies, Rajagopal (2003, 2007) proposed an implicit constitutive relation of the form

$$\boldsymbol{f}(\mathbf{B}, \boldsymbol{\sigma}, \rho) = \mathbf{0}, \tag{5}$$

where ρ is the density of the body. For isotropic bodies, (5) becomes

$$\alpha_0\mathbf{I} + \alpha_1\mathbf{B} + \alpha_2\mathbf{B}^2 + \alpha_3\boldsymbol{\sigma} + \alpha_4\boldsymbol{\sigma}^2 + \alpha_5(\mathbf{B}\boldsymbol{\sigma} + \boldsymbol{\sigma}\mathbf{B}) + \alpha_6(\mathbf{B}\boldsymbol{\sigma}^2 + \boldsymbol{\sigma}^2\mathbf{B})$$
$$+ \alpha_7(\mathbf{B}^2\boldsymbol{\sigma} + \boldsymbol{\sigma}\mathbf{B}^2) + \alpha_8(\mathbf{B}^2\boldsymbol{\sigma}^2 + \boldsymbol{\sigma}^2\mathbf{B}^2) = \mathbf{0}, \tag{6}$$

where α_i $(i = 0, 1, 2, \ldots, 8)$ are scalar functions that depend on the invariants

$$\mathrm{tr}\mathbf{B}, \ \mathrm{tr}\mathbf{B}^2, \ \mathrm{tr}\mathbf{B}^3, \ \mathrm{tr}\boldsymbol{\sigma}, \ \mathrm{tr}\boldsymbol{\sigma}^2, \ \mathrm{tr}\boldsymbol{\sigma}^3, \ \mathrm{tr}(\mathbf{B}\boldsymbol{\sigma}), \ \mathrm{tr}(\mathbf{B}^2\boldsymbol{\sigma}), \mathrm{tr}(\boldsymbol{\sigma}^2\mathbf{B}), \ \mathrm{tr}(\mathbf{B}^2\boldsymbol{\sigma}^2),$$

and the density ρ. For $\|\nabla\mathbf{u}\| \sim O(\delta)$ with $\delta \ll 1$,

$$\mathbf{B} \approx \mathbf{I} + 2\boldsymbol{\varepsilon}. \tag{7}$$

On the other hand, using a Taylor expansion in Cartesian coordinates around $\boldsymbol{\varepsilon} = \mathbf{0}$ and assuming that α_i $(i = 0, 1, 2, \ldots, 8)$ does not depend explicitly on ρ, the following approximation holds:

$$\alpha_i(\boldsymbol{\sigma}, \mathbf{B}) \approx \alpha_i(\boldsymbol{\sigma}, \mathbf{I} + 2\boldsymbol{\varepsilon}) \approx \alpha_i(\boldsymbol{\sigma}) + \left.\frac{\partial\alpha_i}{\partial\varepsilon_{kl}}\right|_{(\boldsymbol{\sigma}, \boldsymbol{\varepsilon}=\mathbf{0})}\boldsymbol{\varepsilon} \quad (i = 0, 1, \ldots, 8). \tag{8}$$

On substituting (7) and (8) into (6), the following implicit relation is obtained for terms up to order δ:

$$\aleph_0\mathbf{I} + \aleph_1\boldsymbol{\varepsilon} + \aleph_2\boldsymbol{\sigma} + \aleph_3\boldsymbol{\sigma}^2 + \aleph_4\boldsymbol{\varepsilon}\boldsymbol{\sigma} + \aleph_5\boldsymbol{\sigma}\boldsymbol{\varepsilon} + \aleph_6\boldsymbol{\varepsilon}\boldsymbol{\sigma}^2 + \aleph_7\boldsymbol{\sigma}^2\boldsymbol{\varepsilon}$$
$$+ (\beth_{0_{kl}}\varepsilon_{kl})\mathbf{I} + (\beth_{1_{kl}}\varepsilon_{kl})\boldsymbol{\sigma} + (\beth_{2_{kl}}\varepsilon_{kl})\boldsymbol{\sigma}^2 = \mathbf{0}, \tag{9}$$

where $\aleph_m = \aleph_m(\boldsymbol{\sigma})$ $(m = 0, 1, \ldots, 7)$ and $\beth_{n_{kl}} = \beth_{n_{kl}}(\boldsymbol{\sigma})$ $(n = 0, 1, 2)$ are (in general) nonlinear scalar and tensor functions of the Cauchy stress tensor $\boldsymbol{\sigma}$. Under certain conditions, (9) can be solved for $\boldsymbol{\varepsilon}$. A simple method to find such conditions is the following. On defining the vector $\epsilon = (\varepsilon_{11}, \varepsilon_{22}, \varepsilon_{33}, 2\varepsilon_{12}, 2\varepsilon_{13}, 2\varepsilon_{23})^{\mathrm{T}}$, (9) can be written as the vector equation

$$\mathsf{M}\epsilon = \mathsf{d}, \tag{10}$$

where the matrix $\mathsf{M} = \mathsf{M}_{6\times6}$ and the vector $\mathsf{d} = \mathsf{d}_{6\times1}$ depend (in general nonlinearly) on $\boldsymbol{\sigma}$. For brevity, the explicit form of M is not shown here. If $\det\mathsf{M} \neq 0$, then $\epsilon = \mathsf{M}^{-1}\mathsf{d}$ can be computed. For isotropic bodies, (5) can be used to obtain the nonlinear relation (Bustamante and Rajagopal, 2010; Bustamante, 2009)

$$\boldsymbol{\varepsilon} = \boldsymbol{g}(\boldsymbol{\sigma}). \tag{11}$$

For an isotropic body that is described by the classical linearized constitutive relation, the function $\boldsymbol{g}(\boldsymbol{\sigma})$ is

$$\boldsymbol{g}(\boldsymbol{\sigma}) = \frac{1}{E}\boldsymbol{\sigma} - \frac{v}{E}(\mathrm{tr}\boldsymbol{\sigma})\mathbf{I}, \tag{12}$$

where E and v are the Young modulus and the Poisson ratio, respectively.

In bodies defined by implicit constitutive relations, the Helmholtz potential can depend on both the stress and the strain (see Rajagopal, 2003, Freed and Einstein, 2013a). When the explicit relation for the stretch **B** in terms of the stress is considered, a potential akin to the complementary potential in classical linearized elasticity theory is obtained. In this work, we consider such a scalar function (Bustamante, 2009) $W = W(\boldsymbol{\sigma})$ such that $\mathbf{g}(\boldsymbol{\sigma}) = \partial W/\partial \boldsymbol{\sigma}$. For isotropic bodies, W is a function of the invariants

$$I_1 = \text{tr}\boldsymbol{\sigma}, \quad I_2 = \frac{1}{2}\text{tr}(\boldsymbol{\sigma}^2), \quad I_3 = \frac{1}{3}\text{tr}(\boldsymbol{\sigma}^3). \tag{13}$$

In Bustamante and Rajagopal (2011) and Ortiz et al. (2012), the following choice was made for the stored energy:

$$W(I_1, I_2) = -\alpha \left[I_1 - \frac{1}{\beta} \ln(1 + \beta I_1) \right] + \frac{\alpha\gamma}{\iota} \sqrt{1 + 2\iota I_2}, \tag{14}$$

where $\alpha, \ \beta, \ \gamma$ and ι are material constant parameters. On substituting (14) into (11) leads to

$$\boldsymbol{\varepsilon} = -\alpha \left[1 - \frac{1}{(1 + \beta I_1)} \right] \mathbf{I} + \frac{\alpha\gamma}{\sqrt{1 + 2\iota I_2}} \boldsymbol{\sigma}. \tag{15}$$

The main feature of W in (14) is that a strain limiting behavior is exhibited for appropriate values of the material constant parameters α, β, γ and ι. As pointed out by Ortiz et al. (2012), these parameters should be obtained from experimental data for materials that exhibit strain limiting behavior and the data corroborated against experiments. In our current work, the material parameters are selected arbitrarily with a view towards determining the versatility or usefulness of these new constitutive relations for elastic bodies.

2.3. Uniaxial tension

Results for a uniaxial tension of a bar are provided to demonstrate the response of an elastic body that is described by the constitutive relation (15). For uniform tension σ applied to the bar, the longitudinal strain is $\varepsilon = \alpha[-1 + 1/(1 + \beta\sigma) + \gamma\sigma/\sqrt{1 + \iota\sigma^2}]$. The following material parameters are chosen:

$$\alpha = 10^{-9}, \quad \beta = 10^{-3}\frac{1}{\text{Pa}}, \quad \gamma = 10\frac{1}{\text{Pa}}, \quad \iota = 10^{-11}\frac{1}{\text{Pa}^2}.$$
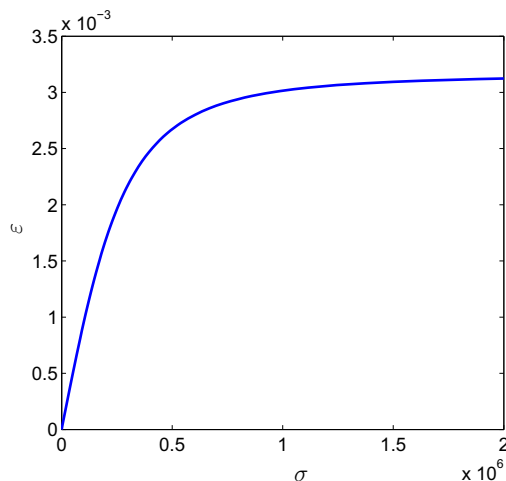
The elastic response of the bar is depicted in Fig. 1.

Fig. 1. Elastic response of a bar under uniaxial tension. The stresses are in Pa.

In the uniaxial tension problem, the parameter ι was observed to have the most significant influence with regard to the response of the elastic body.

2.4. Boundary value problem

Consider an elastic body $\mathcal{B}$ defined by an open bounded domain $\kappa_t(\mathcal{B}) \subset \mathbb{R}^3$ with boundary $\partial \kappa_t(\mathcal{B})$ such that $\partial \kappa_t(\mathcal{B}_u) \cup \partial \kappa_t(\mathcal{B}_t) = \partial \kappa_t(\mathcal{B})$ and $\partial \kappa_t(\mathcal{B}_u) \cap \partial \kappa_t(\mathcal{B}_t) = \emptyset$. The position of a point $x \in \mathcal{B}$ is $\mathbf{x} \in \kappa_t(\mathcal{B})$. A displacement field **u** is sought such that

$$\text{div}\boldsymbol{\sigma} = 0, \tag{16a}$$

where $\boldsymbol{\sigma}$ has to be found from

$$\boldsymbol{\varepsilon} = \frac{\partial W}{\partial \boldsymbol{\sigma}}, \quad \text{where} \quad \boldsymbol{\varepsilon} = \frac{1}{2}\left[\nabla\mathbf{u} + (\nabla\mathbf{u})^{\text{T}}\right]. \tag{16b}$$

In (16b), $\partial W/\partial\boldsymbol{\sigma}$ is in general a nonlinear function of $\boldsymbol{\sigma}$. The boundary conditions are

$$\mathbf{u} = \hat{\mathbf{u}} \quad \text{on } \partial\kappa_t(\mathcal{B}_u), \quad \boldsymbol{\sigma}\mathbf{n} = \hat{\mathbf{t}} \quad \text{on } \partial\kappa_t(\mathcal{B}_t), \tag{16c}$$

where $\hat{\mathbf{u}}$ is an imposed displacement field and $\hat{\mathbf{t}}$ is a prescribed traction.

The foregoing boundary value problem possess exact solutions only for some simple cases (e.g., Bustamante and Rajagopal, 2011, 2012; Rajagopal, 2011b; Rajagopal and Walton, 2011), and presents challenges for the numerical analyst not only because (11) is in general a nonlinear function, but also because the stress $\boldsymbol{\sigma}$ has to be calculated by inversion of (11), if the function is invertible. In general, the study of implicit equations of the form (6) is much more daunting as the balance of mass and linear momentum need to be solved simultaneously with the constitutive equation. In this case, we have to consider as many as ten coupled nonlinear partial differential equations. An additional issue that needs to be taken into account is that $\mathbf{g}$ (or W) should be such that $\|\boldsymbol{\varepsilon}\| \sim O(\delta), \delta \ll 1$ (indeed, $\|\nabla\mathbf{u}\| \sim O(\delta), \ \delta \ll 1$).

3. Finite element method

The solution of the boundary value problem (16) by the finite element method requires a weak form. To this end, we use the principle of virtual work. The following notations are introduced for readability of the weak form:

$$\kappa_t(\mathcal{B}) = \Omega, \quad \partial\kappa_t(\mathcal{B}) = \Gamma, \quad \partial\kappa_t(\mathcal{B}_u) = \Gamma_u, \quad \text{and} \quad \partial\kappa_t(\mathcal{B}_t) = \Gamma_t.$$

3.1. Weak form

Consider trial functions $u_i(\mathbf{x}) \in \mathcal{U} \subset \mathbb{H}^1(\Omega)$ and test functions $\delta u_i(\mathbf{x}) \in \mathcal{V} \equiv \mathbb{H}_0^1(\Omega)$ $(i = 1, 2, 3)$, where $\mathbb{H}^1(\Omega)$ is the Sobolev space of functions with square-integrable first derivatives in Ω, and $\mathbb{H}_0^1(\Omega)$ is the Sobolev space of functions with square-integrable first derivatives in Ω and vanishing values on the essential boundary Γ_u. The weak form (principle virtual work) associated with (16) reads (see for instance Zienkiewicz and Taylor, 2000):

Find $u_i \in \mathcal{U}$ such that

$$\int_{\Omega} \delta\varepsilon_{ij}\sigma_{ij}\,d\Omega - \int_{\Gamma_t} \delta u_i\hat{t}_i\,d\Gamma = 0 \quad \forall \ \delta u_i \in \mathcal{V}, \tag{17}$$

where σ_{ij} is obtained by inversion of the nonlinear implicit relation (11).

3.2. Linearized weak form

Due to the implicit relationship between the strain and the Cauchy stress tensors the weak form becomes nonlinear. The linearization of the weak form can be constructed by approximating the stress field as a two-term Taylor series expansion, $\boldsymbol{\sigma}^{(k)} \approx \boldsymbol{\sigma}^{(k-1)} + \frac{\partial \boldsymbol{\sigma}}{\partial \boldsymbol{\varepsilon}}\big|_{(k-1)} \Delta \boldsymbol{\varepsilon}^{(k)}$, which yields

$$\int_\Omega \delta\varepsilon_{ij} \frac{\partial \sigma_{ij}}{\partial \varepsilon_{kl}}\bigg|_{(k-1)} \Delta\varepsilon_{kl}^{(k)} \, d\Omega = \int_{\Gamma_t} \delta u_i \hat{t}_i \, d\Gamma - \int_\Omega \delta\varepsilon_{ij} \sigma_{ij}^{(k-1)} \, d\Omega, \tag{18}$$

where $\Delta\boldsymbol{\varepsilon}^{(k)}$ is the strain increment associated with an increment in **u**, namely $\Delta\mathbf{u}$, from the step $k-1$ to the step k. Note that in (18), $\partial\boldsymbol{\sigma}/\partial\boldsymbol{\varepsilon}$ is the elasticity tensor and is implicitly computed as

$$\mathcal{C}_{ijkl} = \frac{\partial\sigma_{ij}}{\partial\varepsilon_{kl}} \quad \text{where} \quad \frac{\partial\boldsymbol{\sigma}}{\partial\boldsymbol{\varepsilon}} = \left(\frac{\partial\mathbf{g}}{\partial\boldsymbol{\sigma}}\right)^{-1}. \tag{19}$$

The equality in (19) was obtained by deriving $\boldsymbol{\varepsilon} = \mathbf{g}(\boldsymbol{\sigma})$ with respect to $\boldsymbol{\varepsilon}$ and assuming invertibility of the fourth order tensor $\partial\mathbf{g}/\partial\boldsymbol{\sigma}$. On using (19) along with (15) leads to the following elasticity tensor:

$$\left(\mathcal{C}^{-1}\right)_{ijkl} = \frac{-\alpha\beta}{(1+\beta I_1)} \delta_{ij}\delta_{kl} - \frac{\alpha\gamma\iota}{(1+2\iota I_2)^{3/2}} \sigma_{ij}\sigma_{kl} + \frac{\alpha\gamma}{2\sqrt{1+2\iota I_2}}$$
$$\times (\delta_{ik}\delta_{jl} + \delta_{jk}\delta_{il}). \tag{20}$$

3.3. Discrete linearized weak form

Let the arbitrary test ($\delta\mathbf{u}_h^{(e)}$) element function and the trial ($\Delta\mathbf{u}_h^{(e)}$) element function be

$$\delta\mathbf{u}_h^{(e)}(\mathbf{x}) = \sum_{I=1}^n N_I(\mathbf{x})\delta\mathbf{u}_I^{(e)}, \tag{21a}$$

$$\Delta\mathbf{u}_h^{(e)}(\mathbf{x}) = \sum_{I=1}^n N_I(\mathbf{x})\Delta\mathbf{u}_I^{(e)}, \tag{21b}$$

where N_I's are the finite element shape functions and n is the number of nodes per elements. On using (21), the virtual strains become

$$\delta\boldsymbol{\varepsilon} = \frac{1}{2}\sum_{I=1}^n \left[\delta\mathbf{u}_I^{(e)} \otimes \nabla N_I + \nabla N_I \otimes \delta\mathbf{u}_I^{(e)}\right], \tag{22}$$

whereas the strain increment

$$\Delta\boldsymbol{\varepsilon} = \frac{1}{2}\sum_{I=1}^n \left[\Delta\mathbf{u}_I^{(e)} \otimes \nabla N_I + \nabla N_I \otimes \Delta\mathbf{u}_I^{(e)}\right]. \tag{23}$$

After appealing to the arbitrariness of nodal test functions, assembling the element contributions into the global system, and applying boundary conditions (tractions and displacements) in increments Δt, the following Newton–Raphson scheme is obtained:

$$^{t+\Delta t}\mathsf{K}^{(n-1)}\Delta\mathsf{u}^{(n)} = {}^{t+\Delta t}\mathsf{F} - {}^{t+\Delta t}\mathsf{T}^{(n-1)}, \tag{24}$$

where K is the global tangent stiffness matrix, F and T are the external and internal global nodal force vectors, respectively, and $\Delta\mathsf{u}$ is the column vector that contains all the displacement degrees of freedom of the finite element mesh. On the other hand, $t + \Delta t$ denotes the incremental approach where a solution is known at discrete time t and the solution at discrete time $t + \Delta t$ is sought. Finally, n stands for the equilibrium iterations within an increment. The element contributions are provided in Section 4.

4. Computational implementation

The numerical implementation of the nonlinear theory of implicit elasticity introduces subtle changes into a standard finite element code. The problem at hand is tackled through a

Newton–Raphson scheme. The Newton–Raphson algorithm is given in Box 3.1, where `maxit` stands for the maximum iterations permitted, `tol` $\ll 1$ is a preset Newton's tolerance, `nsteps` are the number of load steps, $\sigma^{(e)}$ is the stress in the element in vector Voigt notation, and $\epsilon^{(e)}$ the strain in the element in vector Voigt notation. To perform the assembly of the element contributions into the global discrete system, the element tangent stiffness matrix and the external and internal element nodal force vectors need to be established. The development of the same is presented in the following subsections, where the plane stress case is considered and 4-node quadrilateral elements are used.

Box 3.1: Newton–Rahpson Solution algorithm.

- INPUT geometry, material parameters: α, β, γ, ι, and solution parameters: `maxit`, `tol`, `nsteps`
- INITIALIZE $u = 0, \Delta u = 0, \sigma^{(e)} = \epsilon^{(e)} = 0$ for all elements
- LOOP over load steps: `step = 1` to `nsteps`
  - INITIALIZE `error = 1.0`, `nit = 0`, `factor = step/nsteps`
  - WHILE (`error` > `tol`) and (`nit` < `maxit`)
    - `nit = nit + 1`
    - FIND K by assembly of the element matrix $\mathsf{K}^{(e)}(\sigma^{(e)})$
    - FIND F by assembly of the element vector $\mathsf{F}^{(e)}$
    - FIND T by assembly of the element vector $\mathsf{T}^{(e)}(\sigma^{(e)})$
    - FIND R = `factor` $\times$ F $-$ T
    - APPLY essential boundary conditions
    - SOLVE $\Delta u = \mathsf{K}^{-1}\mathsf{R}$
    - UPDATE $u = u + \Delta u$
    - UPDATE `error` $= \sqrt{\frac{\Delta u \cdot \Delta u}{u \cdot u}}$
  - END WHILE
- END LOOP

4.1. Stress and strain in the element

For plane stress, the stress and strain in the element in vector Voigt notation are

$$\epsilon^{(e)} = \begin{pmatrix} \varepsilon_{11}^{(e)} & \varepsilon_{22}^{(e)} & 2\varepsilon_{12}^{(e)} \end{pmatrix}^{\mathsf{T}} \tag{25}$$

and

$$\sigma^{(e)} = \begin{pmatrix} \sigma_{11}^{(e)} & \sigma_{22}^{(e)} & \sigma_{12}^{(e)} \end{pmatrix}^{\mathsf{T}}, \tag{26}$$

and they are computed incrementally at a given Gauss point at the Cartesian coordinate $\mathbf{x}_r$ as follows:

$$\epsilon_p^{(e)}(\mathbf{x}_r) = \epsilon_{p-1}^{(e)}(\mathbf{x}_r) + \Delta\epsilon_p^{(e)}(\mathbf{x}_r) \tag{27}$$
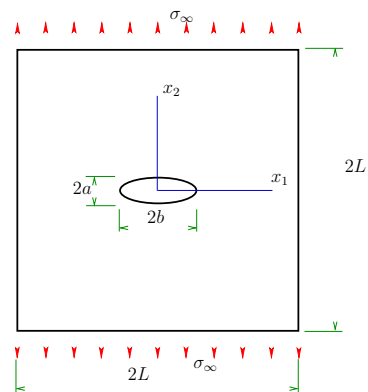

Fig. 2. Plate with an elliptic hole under uniaxial tension.

for the strain in the element, and

$$\sigma_p^{(e)}(\mathbf{x}_r) = \sigma_{p-1}^{(e)}(\mathbf{x}_r) + \Delta\sigma_p^{(e)}(\mathbf{x}_r) \tag{28}$$

for the stress in the element. In (27) and (28), p starts from 1 before the Newton–Rahpson loops initiate. When $p = 1$ it means that the element at the given Gauss point is free of stress and strain, which is part of the second instruction in the algorithm given in Box 3.1. The increments that are involved in the foregoing equalities can be expressed as

$$\Delta\epsilon_p^{(e)}(\mathbf{x}_r) = \sum_{I=1}^{4} \mathsf{B}_I^{(e)}(\mathbf{x}_r)\Delta\mathsf{u}_I^{(e)} \tag{29}$$

and

$$\Delta\sigma_p^{(e)}(\mathbf{x}_r) = \mathsf{C}(\mathbf{x}_r)\Delta\epsilon_p^{(e)}(\mathbf{x}_r), \tag{30}$$

where

$$\mathsf{B}_I^{(e)}(\mathbf{x}_r) = \begin{pmatrix} N_{I,1}(\mathbf{x}_r) & 0 \\ 0 & N_{I,2}(\mathbf{x}_r) \\ N_{I,2}(\mathbf{x}_r) & N_{I,1}(\mathbf{x}_r) \end{pmatrix} \tag{31}$$

is the element nodal strain matrix, and

$$\Delta\mathsf{u}_I^{(e)} = \begin{pmatrix} \Delta u_{I1}^{(e)} \\ \Delta u_{I2}^{(e)} \end{pmatrix} \tag{32}$$

is the element nodal displacement increment. Finally, C is the elasticity tensor in Voigt notation, which for plane stress is obtained from (20) as

$$\mathsf{C} = \begin{pmatrix} \mathcal{C}_{1111} & \mathcal{C}_{1122} & \mathcal{C}_{1112} \\ \mathcal{C}_{1122} & \mathcal{C}_{2222} & \mathcal{C}_{2212} \\ \mathcal{C}_{1112} & \mathcal{C}_{2212} & \mathcal{C}_{1212} \end{pmatrix}. \tag{33}$$

4.2. Internal element nodal force vector

The internal element nodal force vector is expressed as

$$\mathsf{T}^{(e)} = \int_{\Omega^{(e)}} \left(\mathsf{B}_1^{(e)} \quad \mathsf{B}_2^{(e)} \quad \mathsf{B}_3^{(e)} \quad \mathsf{B}_4^{(e)} \right)^{\mathrm{T}} \sigma^{(e)} \, d\Omega, \tag{34}$$

where $\sigma^{(e)}$ is computed as described in Section 4.1 and the integral is numerically solved using Gauss quadrature. The algorithm to compute the internal element nodal force vector is presented in Box 3.2, where *store* instruction means that the quantities need to be saved outside the Newton–Raphson loop for future usage.

Box 3.2: Internal element nodal force vector.

- LOOP over element Gauss points
   - FIND $\sigma^{(e)}$ at the current Gauss point:
      - FIND $\mathsf{C}(\sigma^{(e)})$
      - FIND $\Delta\epsilon^{(e)}$
      - FIND $\Delta\sigma^{(e)}(\mathsf{C}; \Delta\epsilon^{(e)})$
      - UPDATE and STORE $\epsilon^{(e)} = \epsilon^{(e)} + \Delta\epsilon^{(e)}$
      - UPDATE and STORE $\sigma^{(e)} = \sigma^{(e)} + \Delta\sigma^{(e)}$
   - FIND $\mathsf{T}^{(e)}(\sigma^{(e)})$
- END LOOP

4.3. External element nodal force vector

The external element nodal force vector is computed to be

$$\mathsf{F}^{(e)} = \int_{\Gamma_t^{(e)}} \left(N_1^{(e)} \quad N_2^{(e)} \quad N_3^{(e)} \quad N_4^{(e)} \right)^{\mathrm{T}} \hat{\mathbf{t}}^{(e)} \, d\Gamma, \tag{35}$$

where N_I ($I = 1, 2, 3, 4$) is the shape function for a 4-node quadrilateral element, and $\hat{\mathbf{t}}^{(e)} = (\hat{t}_1^{(e)} \ \hat{t}_2^{(e)})^{\mathrm{T}}$ denotes the traction vector applied on an element's edge that is part of the traction boundary. The integral in (35) is also numerically computed using Gauss quadrature.

4.4. Element tangent stiffness matrix

The element tangent stiffness matrix is calculated to be

$$\mathsf{K}^{(e)} = \int_{\Omega^{(e)}} \left(\mathsf{B}_1^{(e)} \quad \mathsf{B}_2^{(e)} \quad \mathsf{B}_3^{(e)} \quad \mathsf{B}_4^{(e)} \right)^{\mathrm{T}} \mathsf{C} \left(\mathsf{B}_1^{(e)} \quad \mathsf{B}_2^{(e)} \quad \mathsf{B}_3^{(e)} \quad \mathsf{B}_4^{(e)} \right) d\Omega, \tag{36}$$

where the integral is numerically evaluated using Gauss quadrature. The algorithm for the element tangent stiffness matrix is provided in Box 3.3, where *store* instruction means that the quantities

Table 1
Ratio a/b for the plate with an elliptic hole.

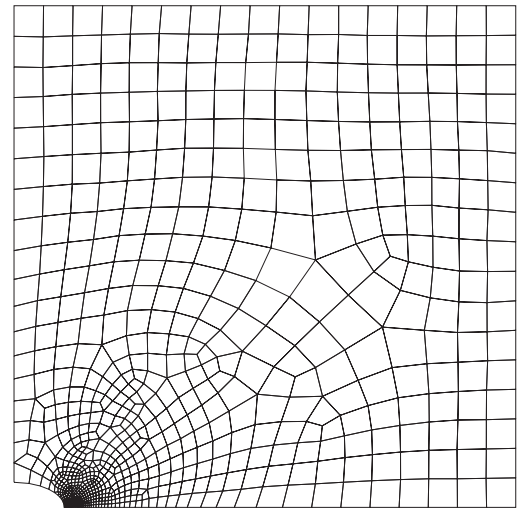| a/b	1	1/2	1/10	1/20

Fig. 3. Mesh for a quarter of the plate with an elliptic hole with $a/b = 1/2$.
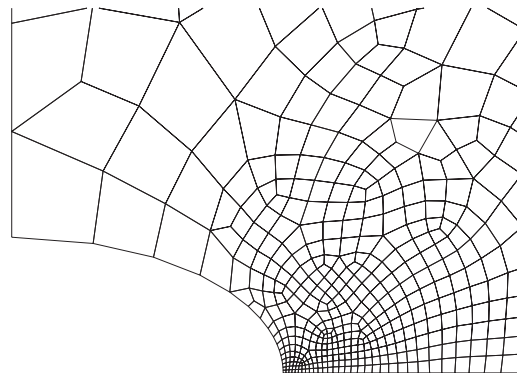

Fig. 4. Detail of the mesh near the point $x_1 = b$, $x_2 = 0$ of the elliptic hole with $a/b = 1/2$.

need to be saved outside the Newton–Raphson loop for future usage.

Box 3.3: Element tangent stiffness matrix.

- LOOP over element Gauss points
  - FIND $\sigma^{(e)}$ at the current Gauss point:
    - FIND $C(\sigma^{(e)})$
    - FIND $\Delta\epsilon^{(e)}$
    - FIND $\Delta\sigma^{(e)}(C; \Delta\epsilon^{(e)})$
    - UPDATE and STORE $\epsilon^{(e)} = \epsilon^{(e)} + \Delta\epsilon^{(e)}$
    - UPDATE and STORE $\sigma^{(e)} = \sigma^{(e)} + \Delta\sigma^{(e)}$
  - FIND $C(\sigma^{(e)})$
  - FIND $K^{(e)}(C)$
- END LOOP

---

5. Numerical examples

In this section, the use of constitutive equations that admit unbounded stresses while strains remain small is demonstrated via two numerical examples. To this end, the constitutive relation (15) is adopted.

In all the computations, the following material constants are used:

$$\alpha = 10^{-9}, \quad \beta = 10^{-3}\frac{1}{\text{Pa}}, \quad \gamma = 10\frac{1}{\text{Pa}}, \quad \iota = 10^{-11}\frac{1}{\text{Pa}^2}.$$

These values differ from those used in Ortiz et al. (2012) (see Eq. (19) therein). The new values of the parameters were chosen to ensure convergence of the Newton–Raphson loops in the examples considered in the present paper.

5.1. Plate with an elliptic hole subjected to uniaxial tension

In this example, a plate with an elliptic hole that is subjected to uniaxial tension is studied (see Fig. 2). Due to symmetry, only a quarter of the plate is considered. The following values for b, L and σ_∞ are chosen for the computations:

$$b = 0.1\,\text{m}, \quad L = 1\,\text{m}, \quad \sigma_\infty = 10^5\,\text{Pa} \quad \text{and} \quad 10^4\,\text{Pa},$$

where, for convergence of the Newton–Raphson loop, two different values for σ_∞ were considered. Table 1 contains the ratio of the
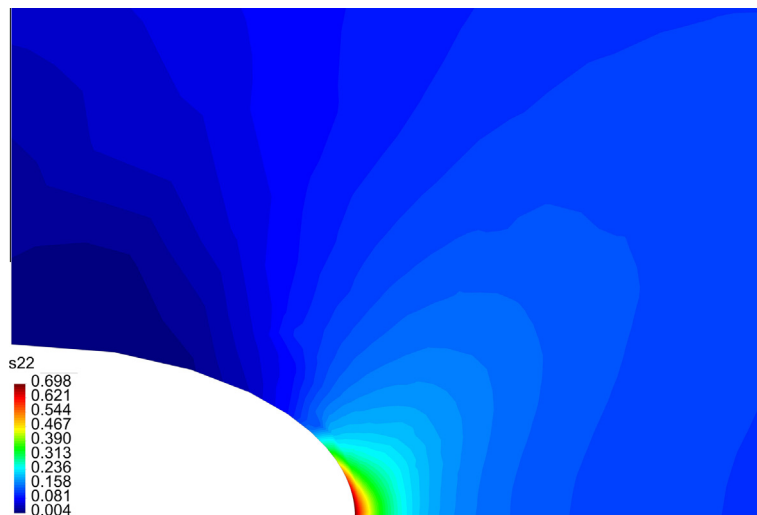
Fig. 5. Contour plot of σ_{22} in MPa near the point $x_1 = b$, $x_2 = 0$ for $a/b = 1/2$.
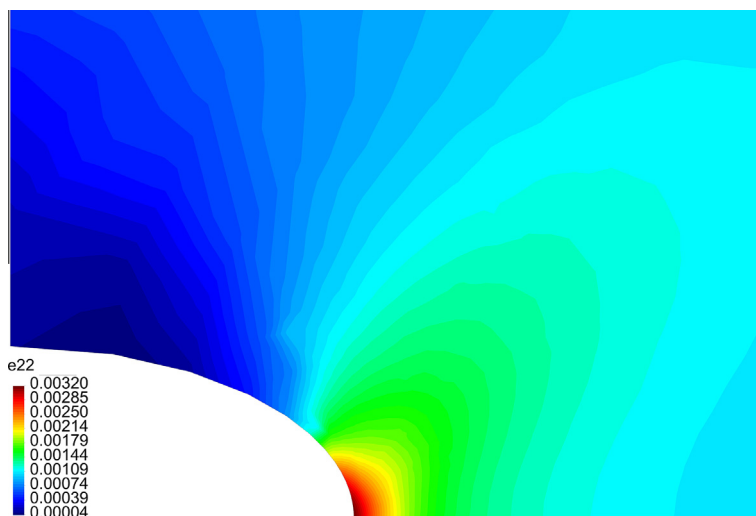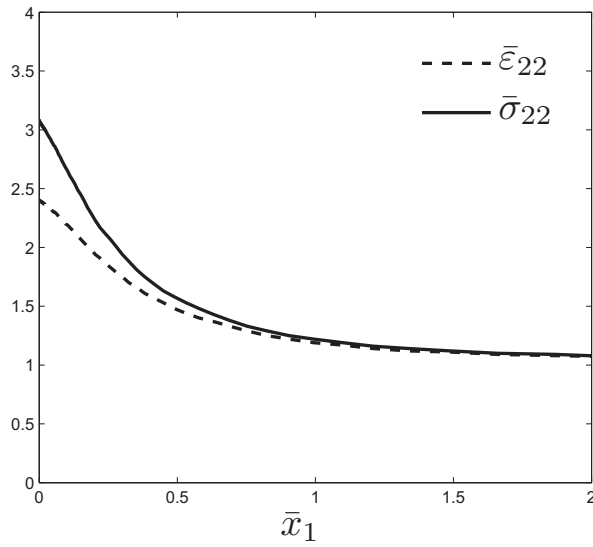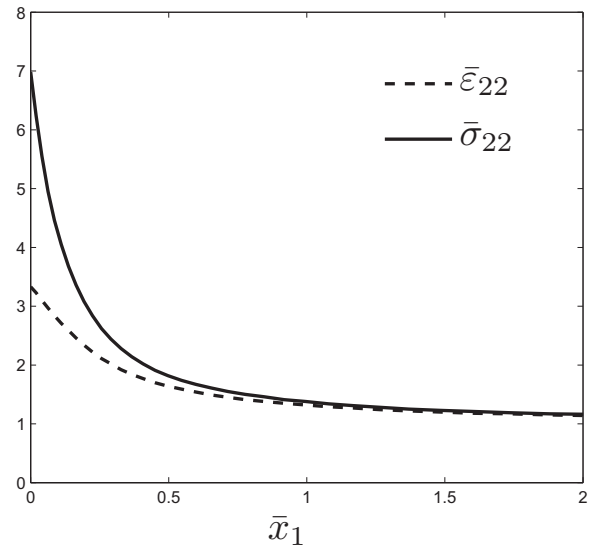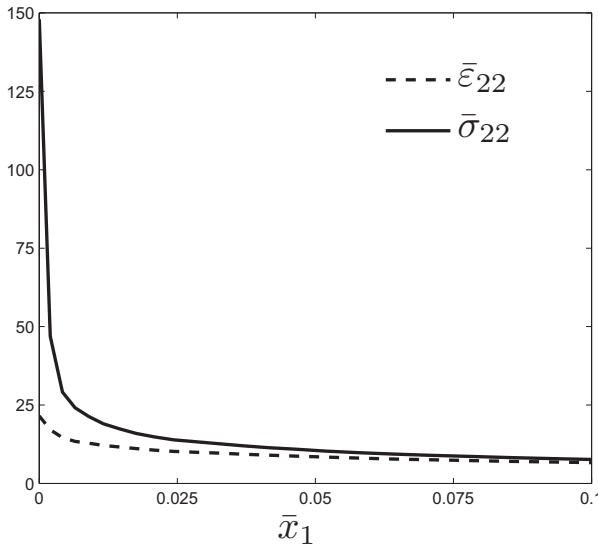

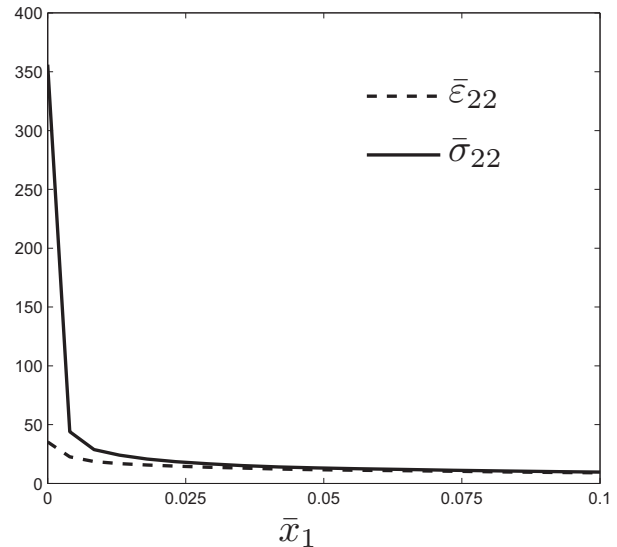**Fig. 6.** Contour plot of ε_{22} near the point $x_1 = b$, $x_2 = 0$ for $a/b = 1/2$.

(a) Case $a/b = 1$, $\sigma_\infty = 10^5$ Pa.

(b) Case $a/b = 0.5$, $\sigma_\infty = 10^5$ Pa.

(c) Case $a/b = 0.1$, $\sigma_\infty = 10^4$ Pa.

(d) Case $a/b = 0.05$, $\sigma_\infty = 10^4$ Pa.

Fig. 7. Normalized stress and normalized strain as functions of $\bar{x}_1$. Stresses and strains are measured on the line $x_2 = 0$, $b \leqslant x_1 < L$ as $b \leftarrow x_1$.
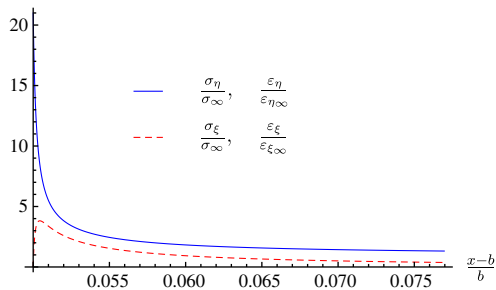

Fig. 8. Normalized stresses and normalized strains as functions of $(x_1 - b)/b$. Results for a plate with an elliptic hole using the classical linearized elasticity theory.

semi-minor axis (denoted by a) to the semi-major axis (denoted by b) of the elliptic holes that were considered in our analyses.

Table 2
Concentration factors for the plate with an elliptic hole under uniaxial tension.

a/b	1	1/2	1/10	1/20
Nonlinear case $\frac{\sigma_\eta}{\sigma_\infty}$	3.09	6.98	148	356
(from Fig. 7) $\frac{\varepsilon_\eta}{\varepsilon_{\eta_\infty}}$	2.41	3.33	21.5	35.2
Linear case Eq. (38)	3	5	21	41

The purpose of this example is to study the qualitative properties of ε_{22} and σ_{22} along the line $x_2 = 0$, $b \leqslant x_1 < L$ as $b \leftarrow x_1$.

A mesh of 4-node quadrilaterals is depicted in Fig. 3 for a quarter of the plate with $a/b = 1/2$. The mesh consists of 835 elements and 898 nodes. Fig. 4 provides a detailed view of the mesh near the point $x_1 = b$, $x_2 = 0$ of the elliptic hole.

The numerical results for σ_{22} and ε_{22} are shown in Figs. 5 and 6 for $a/b = 1/2$ and $\sigma_\infty = 10^5$ Pa. Note that the distributions for σ_{22}

and ε_{22} differ from each other in the sense that the stress concentrates more around the point $x_1 = b$, $x_2 = 0$ than does the strain.

To investigate how stresses and strains behave for different values of the ratio a/b, consider the results presented in Fig. 7, where the following normalized quantities are plotted:

$$\bar{x}_1 = \frac{x_1 - b}{b}, \quad \bar{\sigma}_{22} = \frac{\sigma_{22}}{\sigma_\infty}, \quad \bar{\varepsilon}_{22} = \frac{\varepsilon_{22}}{\varepsilon_{22_\infty}}. \tag{37}$$

It is worth observing that the strain is a non-dimensional quantity. The normalized strain has been considered to recognize that the presence of a hole can lead to an increase (concentration) in the strain field. However, one should bear in mind that although the normalized strain may increase, the absolute strain yet remains small, and more importantly, within the values used for linearizing the strain. In (37), ε_{22_∞} is the component ε_{22} evaluated where the stress σ_∞ is prescribed. The results shown in Fig. 7 suggest that the rate at which the stress increases toward $\bar{x} = 0$ is larger than the rate at which the strain does. Moreover, the difference between the rates increases as a/b gets smaller. Additionally, a stress concentration factor of approximately 350 is observed in Fig. 7(d), whereas for the strain the factor is below 50. This response is expected for an elastic body that is described by a constitutive relation wherein the strains remain small irrespective of the value of the stress.

As a comparison, an exact solution for the plate with an elliptic hole with $L/a \to \infty$ and $L/b \to \infty$ is presented in Fig. 2 in the case of the classical linearized elastic solid. The solution in terms of the elliptic coordinates ξ, η (Timoshenko and Goodier, 1970) is a lengthy expression that depends on ξ, η, c, ξ_0 and σ_∞, which for brevity we do not show here. But we will provide plots for σ_ξ and σ_η for the line $x_2 = 0$, $b \leqslant x_1 < L$ (i.e., for $\eta = 0$) and $a/b = 1/10$. In Fig. 8, plots for the normalized stress components $\sigma_\eta/\sigma_\infty$ and σ_ξ/σ_∞ are depicted. If the exact solution for a linear elastic isotropic body is replaced in (12), it can be shown that the behavior of the normalized strains $\varepsilon_\eta/\varepsilon_{\eta_\infty}$, $\varepsilon_\xi/\varepsilon_{\xi_\infty}$ matches the behavior of the normalized stresses as $x_1 \to b$. From p. 193 of Timoshenko and Goodier (1970), the stress concentration factor $\sigma_\eta/\sigma_\infty$ evaluated at $x_1 = b$ is

$$\frac{\sigma_\eta}{\sigma_\infty} = 1 + 2\frac{b}{a}, \tag{38}$$

which would be the same for $\varepsilon_\eta/\varepsilon_{\eta_\infty}$. Now, an approximate model of a plate with a crack under a traction field that is sufficiently far away (i.e., a crack under mode I) is obtained for $a \ll b$. On using (38), $\sigma_{22}(x_1 \to b)/\sigma_\infty = \sigma_\eta/\sigma_\infty \to \infty$ if $a/b \to 0$. The same behavior would be observed for $\varepsilon_{22}/\varepsilon_{22_\infty}$, which is physically impossible for linearized elastic bodies. On the contrary, with the use of constitutive relations of the form given in (11), appropriate expressions of g can be found such that the stresses are large (possibly unbounded) while strains remain small as $x_1 \to b$ irrespective of the value of the stress.

Table 2 summarizes the approximate concentration factors that are inferred from the numerical results of Fig. 7. The reference values obtained from (38) for the classical theory of elasticity are also provided for comparison. We once again observe that one should not conclude erroneously that the strains are becoming large by simply judging from the values of the normalized strain given for the nonlinear model in Table 2. This is not the case; the strains remain limited within the bounds for which linearization is valid. The normalized strain essentially is the ratio of two strains, both of which are sufficiently small, but one much larger than the other.

5.2. Stepped flat tension bar with shoulder fillets

In this example, the elastic response of a stepped flat tension bar with shoulder fillets (Young and Budynas, 2002; Pilkey, 1997) is studied. This plane stress problem is depicted in Fig. 9(a), where a uniform tension σ_∞ is applied on the right side of the plate, while the left edge is fixed in the axial direction. The radius of the shoulder fillet is denoted by r. For $r = 0$, unbounded stresses and strains would be predicted in the shoulder fillet by the classical linearized theory of elasticity, thereby contradicting the assumption within which the model is derived. A detailed view of the shoulder fillet is shown in Fig. 9(b).

The following dimensions are assumed for the stepped flat tension bar:
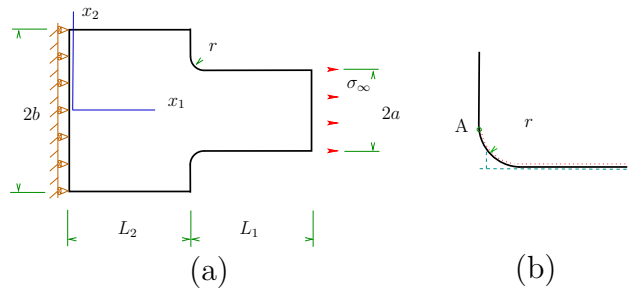

Fig. 9. Stepped flat tension bar with shoulder fillets.

Table 3
Values for the radius of the shoulder fillet, in meters.

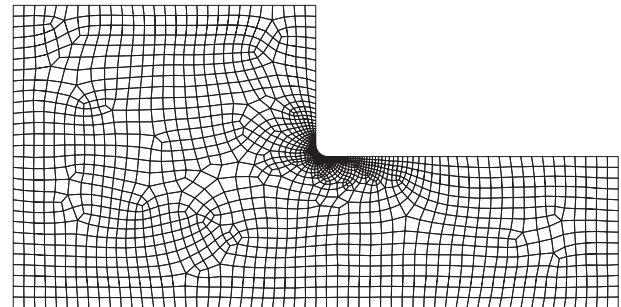| r	0.04	0.02	0.01	0.004	0.002

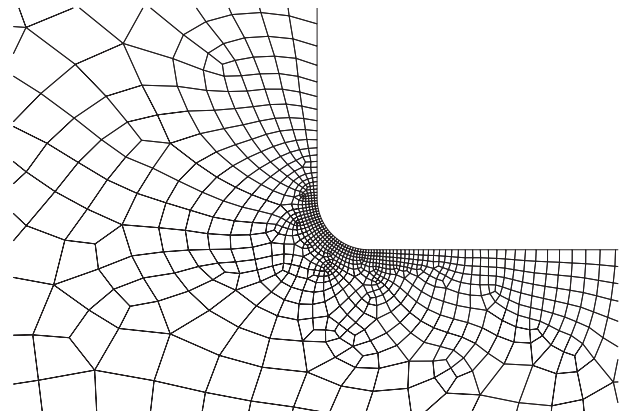**Fig. 10.** Mesh used for the stepped flat tension bar with shoulder fillets of $r = 0.02$.

Fig. 11. Detail of the mesh at the shoulder fillet of the stepped flat tension bar with $r = 0.02$.

$a = 0.5\,\text{m}, b = 1\,\text{m}, L_1 = 0.5\,\text{m}, L_2 = 0.5\,\text{m},$

$\sigma_\infty = 10^5\,\text{Pa} \quad \text{and} \quad 5 \times 10^4\,\text{Pa},$

whereas the values for r are presented in Table 3.

Due to symmetry, only a half of the plate is considered. Figs. 10 and 11 provide details of the mesh used for the plate with $r = 0.02$. Contour plots for σ_{11} and ε_{11} are presented in Figs. 12 and 13 for the plate with $r = 0.02$. From these figures, a high stress concentration is observed near the shoulder of the fillet. The results show that the strain tends to be bounded as the stress increases. Furthermore, consider the results shown in Fig. 14, where $\bar{\varepsilon}_{11}$ and $\bar{\sigma}_{11}$ are plotted as functions of $\bar{x}_1$ for an horizontal line (see Fig. 9(a)) defined by $x_2 = a$, $L_2 < x_1 < L_1 + L_2$. The normalized strain ($\bar{\varepsilon}_{11}$) and the normalized stress ($\bar{\sigma}_{11}$) are defined as in (37), whereas the normalized distance is $\bar{x}_1 = (x_1 - L_2)/r$. In Fig. 14, $\bar{\varepsilon}_{11}$ and $\bar{\sigma}_{11}$ are measured along the line that defines the shoulder fillet starting at point A (see Fig. 9(b)), then toward the right. However, only the position x_1 along this line is used to compute $\bar{x}_1$. Exact solutions for the stepped flat tension bar with shoulder fillets are not available. However, approximate expressions for the stress concentration

factor can be found, for instance, in Table 17.1 on p. 784, Section 50 of Young and Budynas (2002); Figure 106, chapter 3 of Timoshenko and Goodier (1970); Chart 3.1 on p. 150 of Pilkey (1997); and in the original work of Weibel (1934).

In the plots presented in Fig. 14, the concentration of stresses and strains occurs near the normalized position $\bar{x}_1 = 0.5$, which is the location of a point near the middle of the shoulder fillet. The same is inferred from the contour plots presented in Figs. 12 and 13.

The results shown in Fig. 14 suggest that the rate at which the stress increases toward $\bar{x}_1 = 0.5$ is larger than the rate at which the strain does, and the difference between the rates increases as r gets smaller. Furthermore, the concentration factor for the stress can be quite large, whereas for the strains it remains small. This response is consistent with the kinematics of small deformations.

Approximate concentration factors that are inferred from our numerical results of Fig. 14 are compared with approximate values obtained from the classical theory of linearized elasticity (see Chart 3.1 on p. 150 of Pilkey, 1997). This comparison is presented in Table 4.
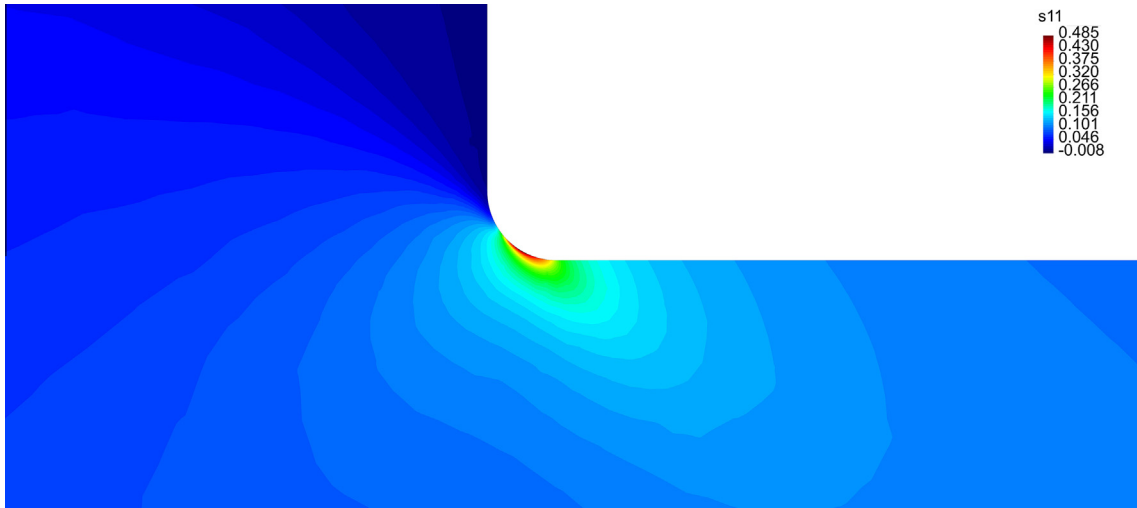

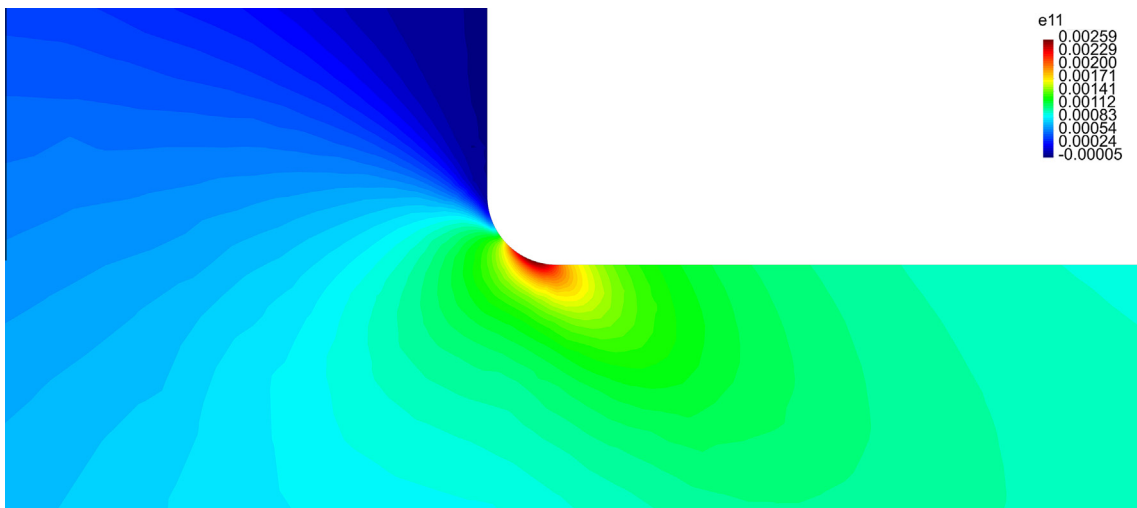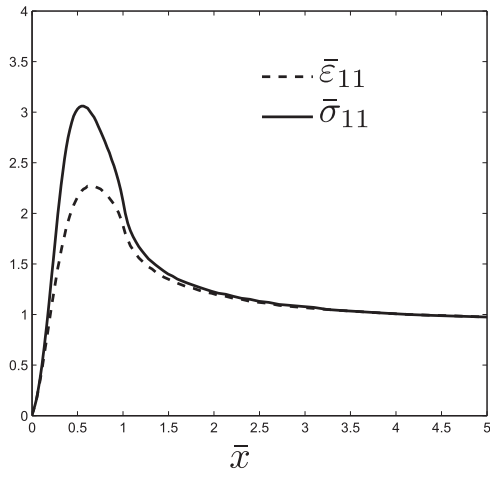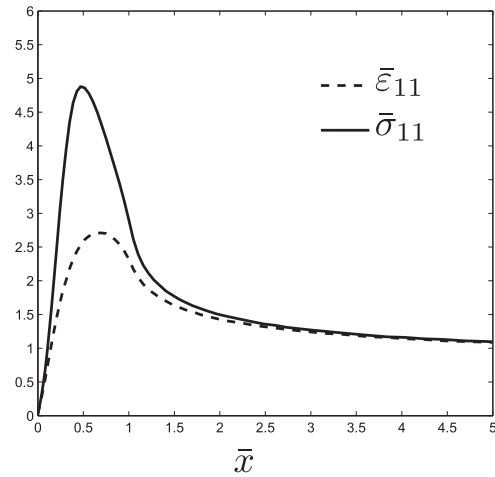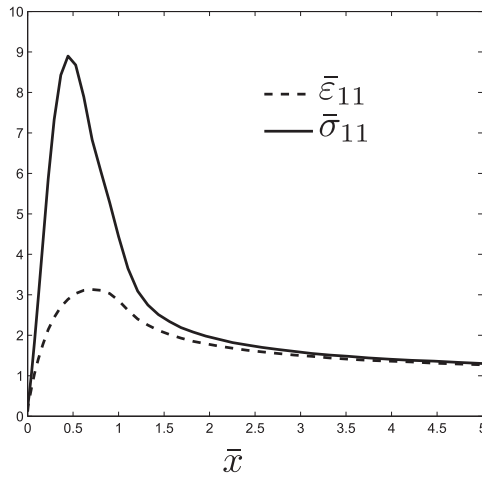**Fig. 12.** Contour plot for σ_{11} MPa near the fillet with $r = 0.02$.

Fig. 13. Contour plot for ε_{11} near the fillet with $r = 0.02$.
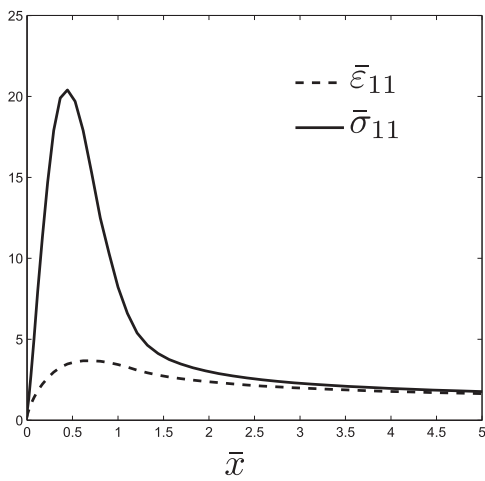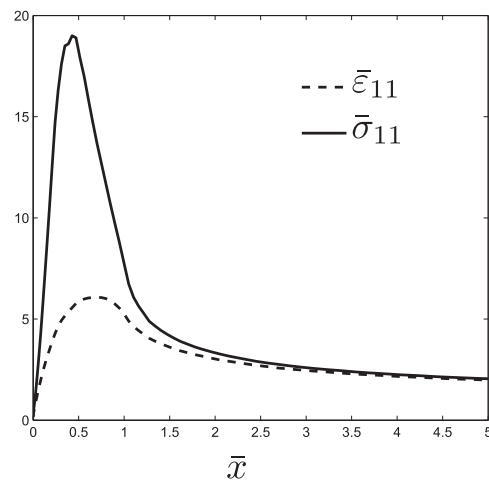
Fig. 14. Stepped flat tension bar with various shoulder fillets. Normalized stress and normalized strain as functions of the normalized distance $\bar{x} = (x - L_2)/r$.

Table 4
Concentration factors for the stepped flat tension bar with shoulder fillets.

$r/(2a)$	0.04	0.02	0.01	0.004
Nonlinear case $\frac{\sigma_{11}}{\sigma_\infty}$	3.06	4.88	8.9	20.4
(from Fig. 14) $\frac{\varepsilon_{11}}{\varepsilon_{11\infty}}$	2.27	2.71	3.13	3.67
Linear case	3.2	3.8	4.5	> 5

Acknowledgments

References

Bulíček, M., Málek, J., Rajagopal, K.R., Walton, J.R., 2013. Existence of solutions for the anti-plane stress for a new class of 'strain-limiting' elastic bodies, submitted for publication.

Bustamante, R., 2009. Some topics on a new class of elastic bodies. Proc. R. Soc. A 465, 1377–1392.

Bustamante, R., Rajagopal, K.R., 2010. A note on plain strain and stress problems for a new class of elastic bodies. Math. Mech. Solids 15, 229–238.

Bustamante, R., Rajagopal, K.R., 2011. Solutions of some simple boundary value problems within the context of a new class of elastic materials. Int. J. Non-linear Mech. 46, 376–386.

Bustamante, R., Rajagopal, K.R., 2012. On the inhomogeneous shearing of a new class of elastic bodies. Math. Mech. Solids 17, 762–778.

Bustamante, R., Rajagopal, K.R., 2013. On a new class of electro-elastic bodies. ii. Boundary value problems. Proc. R. Soc. A, 469. http://dx.doi.org/10.1098/rspa.2013.0106.

Bustamante, R., Rajagopal, K.R., 2013. On a new class of electroelastic bodies. i. Proc. R. Soc. A, 469. http://dx.doi.org/10.1098/rspa.2012.0521.

Freed, A.D., Einstein, D.R., 2013a. An implicit elastic theory for lung parenchyma. Int. J. Eng. Sci. 62, 31–47.

Freed, A.D., Einstein, D.R., 2013. Membrane theory of implicit elasticity, submitted for publication.

Freed, A.D., Liao, J., Einstein, D.R., 2013. A membrane model from implicit elasticity theory: application to visceral pleura. Biomech. Model Mechanobiol, in press. http://dx.doi.org/10.1007/s10237-013-0542-8.

Kulvait, V., Málek, J., Rajagopal, K.R., 2013. Anti-plane stress state of a plate with a v-notch for a new class of elastic solids. Int. J. Fract. 179, 59–73.

Ortiz, A., Bustamante, R., Rajagopal, K.R., 2012. A numerical study of a plate with a hole for a new class of elastic bodies. Acta Mech. 223, 1971–1981.

Pilkey, W.D., 1997. Peterson's Stress Concentration Factors, second ed. John Wiley & Sons, NY.

Rajagopal, K.R., 2003. On implicit constitutive theories. Appl. Math. 48, 279–319.

Rajagopal, K.R., 2007. The elasticity of elasticity. Z. Angew. Math. Phys. 58, 309–317.

Rajagopal, K.R., 2011a. Conspectus of concepts of elasticity. Math. Mech. Solids 16, 536–562.

Rajagopal, K.R., 2011b. Non-linear elastic bodies exhibiting limiting small strain. Math. Mech. Solids 16, 122–139.

Rajagopal, K.R., Srinivasa, A.R., 2007. On the response of non-dissipative solids. Proc. R. Soc. A 463, 357–367.

Rajagopal, K.R., Srinivasa, A.R., 2009. On a class of non-dissipative solids that are not hyperelastic. Proc. R. Soc. A 465, 493–500.

Rajagopal, K.R., Walton, J.R., 2011. Modeling fracture in the context of strain-limiting theory of elasticity: a single anti-plane crack. Int. J. Fract. 169, 39–48.

Timoshenko, S.P., Goodier, J.N., 1970. Theory of Elasticity, third ed. McGraw-Hill, NY.

Weibel, E.E., 1934. Studies in photoelastic stress determination. Appl. Mech. Sect. 56, 637–658.

Young, W.C., Budynas, R.G., 2002. Roark's Formulas for Stress and Strain, seventh ed. McGraw-Hill, NY.

Zienkiewicz, O.C., Taylor, R.L., 2000. The finite element method, . The Basis, Fifth ed., vol. 1. Butterworth-Heinemann, Oxford, UK.